Journal of Materials Chemistry

PAPER

Multi-photon *in situ* synthesis and patterning of polymer-embedded nanocrystals†

Andrea Camposeo,[*a] **Marco Polo,**[a] **Antonio A. R. Neves,**[a] **Despina Fragouli,**[b] **Luana Persano,**[a] **Sandra Molle,**[a] **Anna M. Laera,**[c] **Emanuela Piscopiello,**[c] **Vincenzo Resta,**[c] **Athanassia Athanassiou,**[abd] **Roberto Cingolani,**[d] **Leander Tapfer**[c] **and Dario Pisignano**[*abe]

The *in situ* synthesis and patterning of CdS nanocrystals in a polymer matrix is performed *via* multi-photon absorption. Quantum-sized CdS nanocrystals are obtained by irradiating a cadmium thiolate precursor dispersed in a transparent polymer matrix with a focused near infrared femtosecond laser beam. High resolution transmission electron microscopy evidences the formation of nanocrystals with wurtzite crystalline phase. Fluorescent, nanocomposite patterns with sub-micron spatial resolution are fabricated by scanning the laser beam on the polymer–precursor composite. Moreover, the emission energy of the CdS nanocrystals can be tuned in the range 2.5–2.7 eV, by changing the laser fluences in the range 0.10–0.45 J cm^{-2}. This method enables therefore the synthesis of luminescent, CdS-based composites to be used within patterned nanophotonic and light-emitting devices.

Introduction

Organic–inorganic nanocomposites are widely exploited in different fields because of the possibility of tailoring their properties by properly combining the constituents.[1] These materials may comprise a polymer host doped with metallic or semiconductor nanoparticles, and combine the advantages of organics in terms of processing with the catalytic, electronic and optical properties of nanocrystals.[1] Among different fillers, CdS quantum dots are largely used due to their size-dependent optical properties, *i.e.* band gap energy tunable from UV to visible.[2,3] CdS-based nanocomposites find, therefore, application in quantum dot sensitized solar cells[4] and as high-efficiency emitting materials.[5]

Synthesis approaches play a central role in controlling the particles size and their distribution in the polymer, thus determining the resulting physico-chemical properties of the nanocomposites.[6] Many methods are based on producing nanoparticles independently from the host, and on subsequently embedding them into the matrix upon mechanical mixing (*ex situ*).[7] An alternative approach (*in situ*) consists in forming nanoparticles directly into the polymer[8] by thermal,[9] chemical,[10] or optical[11,12] decomposition of suitable precursors.[13] This may offer a superior control on the dispersion of particles, and in principle allows one to tailor their size through the process temperature[9] or reaction time.[14] Unfortunately, thermally and chemically assisted *in situ* synthesis often needs specific temperature and atmosphere conditions, and hardly allows the nanoparticles formation to be restricted within limited regions of samples to obtain chemical or physical patterns. However, since the optical properties of nanocomposites are strongly affected both by the particle size and by eventual micro/nanostructures,[15] methods for generating patterns of size-controlled nanoparticles are highly desirable. To this aim, developed multi-step processes include sequential synthesis of a radiation-sensitive material containing suitable precursors, patterning by standard lithographies and final *in situ* growth of nanoparticles.[16] The high level of complexity of multi-step procedures may however limit their applicability.

Single-step synthesis in pre-defined regions can be carried out by UV-based methods by photolithography.[12] Alternatively, the use of focused laser beams, similarly to laser writing based on one- or two-photon absorption,[17] has the potential to effectively localize the formation of nanoparticles in the matrix, which is not achieved by conventional techniques. In particular, high fluence fs-laser beams inducing multiphoton absorption can also activate particles formation with sub-micron resolution, thus enabling the concomitant growth of nanocrystals and patterning within the same process.

[a]National Nanotechnology Laboratory, Istituto Nanoscienze-CNR, via Arnesano, 73100 Lecce, Italy. E-mail: andrea.camposeo@nano.cnr.it
[b]Center for Biomolecular Nanotechnologies, Istituto Italiano di Tecnologia@UNILE, via Barsanti 1, I-73010 Arnesano, LE, Italy
[c]ENEA, Technical Unit "Material Technology" Research Centre of Brindisi (UTTMATB), S.S. 7 Appia km 706, I-72100 Brindisi, Italy
[d]Istituto Italiano di Tecnologia (I.I.T.), via Morego 30, I-16163 Genova, Italy
[e]Dipartimento di Matematica e Fisica "Ennio De Giorgi", Università del Salento, via Arnesano, I-73100 Lecce, Italy. E-mail: dario.pisignano@unisalento.it
† Electronic supplementary information (ESI) available. See DOI: 10.1039/c2jm16625a

In this paper, we report on simultaneous *in situ* synthesis of CdS nanoparticles and patterning *via* multi-photon absorption. Quantum-sized CdS nanocrystals are obtained by irradiating cadmium thiolate precursors [Cd(SC$_{12}$R$_{25}$)$_2$] (C12) dispersed in a transparent polymer matrix (TOPAS®) with a focused near infrared laser beam. The advantages of this approach include the controlled CdS growth in a microscale volume within the polymeric matrix, and the possibility of tuning the optical properties of nanoparticles by modulating the laser beam properties. CdS nanocrystals with emission tunable in the range 2.5–2.7 eV are obtained for laser fluences in the range 0.10–0.45 J cm^{-2}.

Materials and methods

TOPAS®, a cyclic olefin copolymer derived from ethylene and norbornene units, is used as a polymer matrix. This thermoplastic polymer is particularly suited for light-emitting composites, being optically transparent in the visible and near infrared range. Furthermore, TOPAS® displays a low water absorption and good chemical resistance to hydrolysis, acids and organic polar solvents.[18] The unimolecular cadmium thiolate precursors for the synthesis of CdS are prepared by following the procedure reported in ref. 9b. Briefly, the cadmium bis-dodecanethiolate precursors (C12) are synthesised by using the cadmium nitrate hexahydrate (Cd(NO$_3$)$_2$·6H$_2$O) salt as the starting reagent. This salt is initially suspended in toluene and then dissolved by adding an aqueous solution of ammonium hydroxide (25 wt%). The product precipitates in the reaction medium immediately after adding the dodecanethiol. The white precipitate is separated from solution by filtration and dried under vacuum. The compositional analysis of the Cd(SC$_{12}$H$_{25}$)$_2$, carried out by elemental analysis, shows C, H, and S contents of 55.7%, 10% and 12.3% respectively, in good agreement with the expected values (C, H, S, 56.0%, 9.7%, 12.4%). Cadmium nitrate, dodecanethiol and toluene are purchased from Aldrich, and are used without further purification. To obtain nanocomposite films, C12 (200 mg) is dispersed in a solution of TOPAS® (800 mg) in toluene (10 ml). The thiolate–polymer mixture is sonicated for 30 min in order to obtain the maximum dispersion of the insoluble metal thiolate. Finally, the TOPAS®–C12 films are prepared through three successive spin coatings on both glass cover-slip and Si substrates at 1600 rpm for 60 s. Photoluminescence (PL) characterization of these pristine films does not evidence any emission signal typical of CdS, therefore ruling out any nanoparticle formation due to the film processing. Finally, the crystallographic structure and ordering within the polymer matrix of the precursor are analyzed by means of a Philips PW1880 3 kW Bragg–Brentano X-ray diffractometer (Cu-Kα radiation, λ = 1.54 Å).

Laser-assisted synthesis and patterning

A direct laser writing technique is exploited for texturing the nanocomposite films. Laser pulses emitted by a fs-system (Mira, Coherent: peak wavelength 800 nm, pulse width of 200 fs, repetition rate of 76 MHz) are strongly focused on the sample surface through the glass substrate, by using the high numerical aperture (NA = 1.3) oil immersion objective lens of

an inverted microscope (Axiovert 40, Zeiss). The samples are mounted on a computer-controlled piezoelectric stage (P-563.3CD, Physik Instrument), capable of 3-dimensional scanning with a 300 μm range on each axis. By moving the piezostage *via* a dedicated software, the CdS nanoparticles growth is induced in pre-defined patterns. Alternatively, sample irradiation is performed by using a fs laser system composed of a regenerative amplifier (Legend, Coherent, λ = 800 nm, pulse width 180 fs, repetition rate 1 kHz, beam diameter 6 mm). By this way, larger areas of the nanocomposite films (~1 cm^2) can be exposed. The beam is focused on the sample surface by a cylindrical lens (f = 100 mm). The laser fluence incident on the sample surface is adjusted by a set of neutral density filters. The samples are mounted on a micrometric manual stage in order to expose a continuous pattern constituted by adjacent stripes, each having an area of about 2 × 10^{-2} mm^2.

Morphological and optical characterization

TEM measurements are performed by using a TECNAI F30 microscope operating at 300 kV and a point-to-point resolution of 0.205 nm. For the TEM specimen preparation, the nanocomposite films, realized by exposing TOPAS®–C12 to the femtosecond laser beam, are carefully removed from the Si-substrate and then dissolved in chloroform, soon after the laser exposure. In this way, effects related to eventual interactions between the electron beams with precursors are ruled out. Finally, a small amount of the solution is dropped on a copper grid and dried.

Atomic Force Microscopy (AFM) is performed by a multimode head (Veeco) equipped with a Nanoscope IIIa controller (Veeco), operating in tapping mode. Si cantilevers with a resonant frequency of about 300 kHz are used to image the film surface after laser irradiation.

Optical characterization. Fluorescence micrographs are acquired by a MZ16FA Leica stereomicroscope equipped with a mercury lamp. The PL spectra are collected by a confocal microscopy system. Spatially resolved PL measurements are performed on the irradiated films by a confocal microscope (Leica, TCS-SP5). The irradiated areas are investigated by using an excitation laser with a wavelength of 405 nm, focussed on the samples through a 40× oil immersion objective with a numerical aperture (N.A.) of 0.7. The PL measurements at variable temperature are performed by mounting the samples in a He closed-cycle cryostat under vacuum (10^{-4} mbar) and exciting the samples by a cw He–Cd laser (λ = 325 nm). The emission is collected by a fiber-coupled monochromator (Jobin Yvon, mod. iHR320) equipped with a charge-coupled device (CCD, Jobin Yvon, Symphony).

Time resolved PL measurements are performed in single photon counting mode by exciting the samples at λ = 296 nm, with a repetition rate of 1 MHz. The time resolution is estimated around 0.5 ns. The photo-stability of the nanocomposite emission is characterized by continuously exciting the samples with a pulsed UV laser (Q-switched Nd:YAG laser, Spectra Physics) in air and collecting the emission spectra at regular time intervals.

Results and discussion

Polymer-precursors characterization

We investigate the morphology of the TOPAS®–C12 films used for the multi-photon synthesis by atomic force microscopy (Fig. 1a). The surface roughness (root mean square, RMS) is about 170 nm, mainly due to the presence of microscale aggregates of precursor molecules (bright regions of Fig. 1a). In fact, in thiolate precursors with long chain thiols (number of C atoms ≥ 12) the chain–chain interaction may favor the formation of periodic lamellar structures (superlattice structures, scheme in Fig. 1b).[9b] Experimental evidence of the lamellae is given by wide-angle X-ray scattering spectra (Fig. 1c) exhibiting super-lattice peaks corresponding to a periodicity along the chain direction, $D_L = 35$ Å. This value agrees very well with the calculated molecule length obtained by considering the projection of the bond length of the C atoms along the molecule main
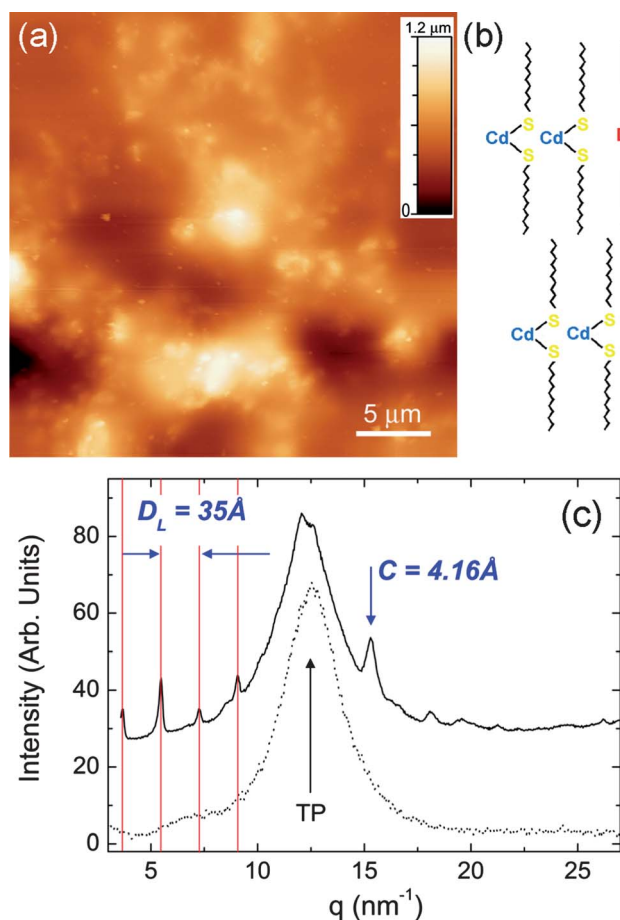
axis and also taking into account the atomic diameters of S and Cd ($D_{th} = 35.5$ Å).[9b] The Bragg peak observed at $q = 15$ nm^{-1} may be related to the Cd–Cd distance (perpendicular to the chain direction) and corresponds to about 4.1 Å.

We preliminarily evaluate the impact of the formation of nanocrystals on the system rheology, an important issue for the structural stability, patterning and processability of the resulting material. To this aim, the nanocrystals are synthesized *in situ* by the standard thermal treatment at 250 °C for 20 minutes.[9b] We notice a shear-thinning behaviour in all the investigated frequency range (Fig. S1 of the ESI†). More importantly, the enhancement of the system viscosity (η) as a consequence of nanoparticles formation is found by rotational viscosimetry for frequencies (ω) values between 10^{-2} and 10^2 s^{-1}. With respect to pristine samples, η increases by about 10 to 70% after nanocrystal formation (depending on the shear-rate). This result suggests that patterning by conventional methods such as nanoimprinting or soft molding after the *in situ* synthesis of nanoparticles would be difficult because of the higher material viscosity. This motivation is at the base of our seeking for alternative, multi-photon methods for spatially selective synthesis and patterning of the nanocomposite.

Nanocomposite synthesis and patterning

Nanocomposite samples are produced by laser irradiation of polymer-precursor films with a pulsed fs-system ($\lambda = 800$ nm, scheme of the set-up in Fig. 2). The TOPAS®–C12 films display an absorption peak at about 266 nm, whereas they are transparent at the relevant wavelength used for the nanocomposite synthesis (Fig. 2).

Therefore, given the negligible linear absorption of the C12 precursor molecules and the polymer matrix at the laser wavelength (Fig. 2), the energy-delivery to samples has to be mediated by multi-photon processes. Indeed, we measure for our system a transmission decrease of about 15% by increasing the incident laser power to values of the order of 10 of GW mm^{-2}, which indicates a clear absorption enhancement at high exposure fluences for the off-resonant (800 nm) wavelength. The resulting
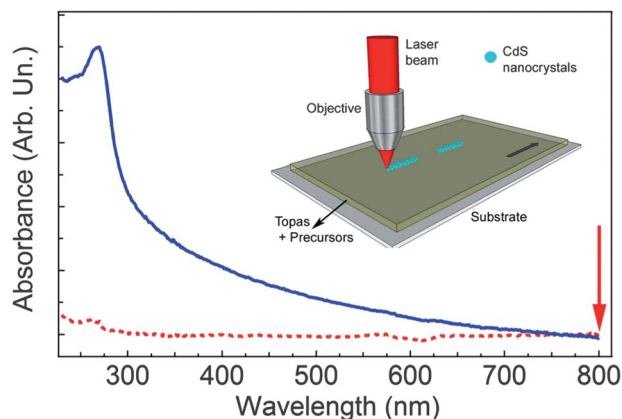

Fig. 1 (a) AFM topographic image of the TOPAS®–C12 film before laser exposure. Bright regions correspond to the C12 precursors, forming a lamellar structure with a unit cell schematized in (b). (c) Experimental wide-angle X-ray scattering spectrum of the C12 molecular precursor dispersed in TOPAS polymer. The superlattice peaks (highlighted by red vertical lines) indicate a regular arrangement of the C12 molecules of lamellar periodicity of 35 Å. The Bragg peak located at $q = 15$ nm^{-1} is attributed to the Cd–Cd distance between the precursor chains, whereas the broad peak (TP) is due to the amorphous polymer scattering, as shown by the dotted line.

Fig. 2 Absorption spectra of the TOPAS®–C12 films (continuous line). The absorption of TOPAS® is also shown for comparison (dotted line). The arrow indicates the exposure laser wavelength ($\lambda = 800$ nm). Inset: schematics of the laser writing system.

formation of CdS nanoparticles is clearly appreciable by high-resolution transmission electron microscopy (HRTEM, Fig. 3). Phase contrast imaging highlights the presence of nanocrystals in the regions exposed to fs-laser pulses by pronounced lattice fringes (Fig. 3). The particles exhibit a spherical shape and hexagonal symmetry (wurtzite structure) as confirmed by fast Fourier transform analysis (Fig. 3b). The average particle size is estimated to be 4 nm.

A further evidence of the nanocrystal growth is provided by the photoluminescence of the irradiated areas, which shows the characteristic emission peak of CdS nanoparticles at about 2.4 eV, only after the exposure to the writing laser (Fig. 4a). Negligible emission is instead measured in the TOPAS®–C12 samples after solution and film processing. Furthermore, we investigate the effects of the exposure to the fs laser pulses on the surface topography, by performing an AFM analysis at the edge of an exposed region. Data displayed in Fig. 4b and c do not evidence any significant variation of the polymer volume after laser irradiation. These results allow ruling out the eventual
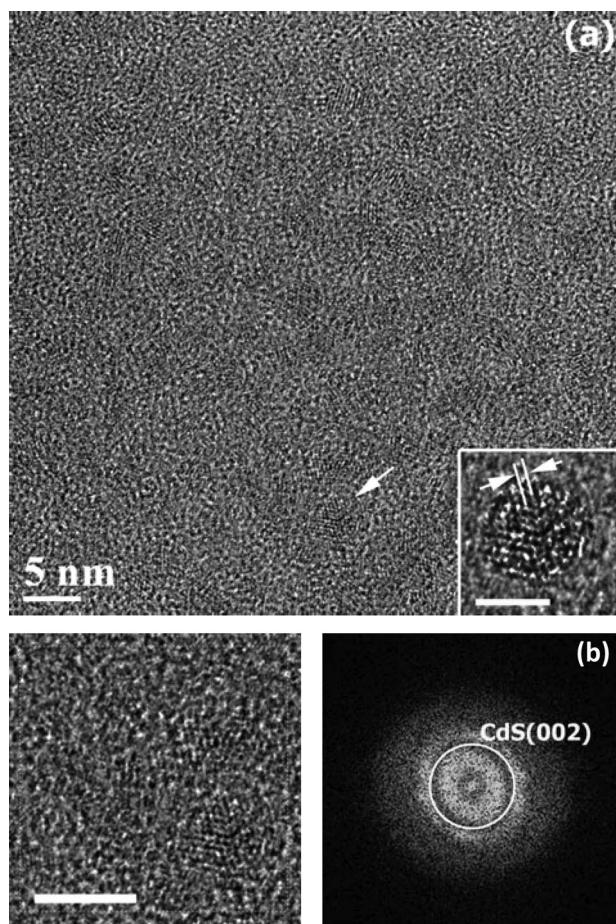

Fig. 4 (a) PL spectrum of the composite film, from regions exposed to the fs laser beam (continuous line) and from un-exposed regions (dashed line). AFM topographic image (b) and height profile (c) of the nanocomposite film after laser exposure. The micrograph is collected at the edge of an exposed area, marked by the continuous line. (d and e) PL micrographs of realized patterns, obtained by scanning the focused laser at 200 μm s^{-1} with an incident fluence of 0.2 J cm^{-2}. (f and g) Confocal fluorescence micrographs of other patterns, realized following the same experimental procedure.

ablation of the polymer matrix, even at the highest exposure fluences (0.7 J cm^{-2}). We conclude that patterning of the nanocomposite films through the spatially localized, *in situ* growth of CdS nanoparticles leads to non-morphological structures. These are in principle advantageous for micropatterned light-emitting devices, as they are fully compatible with the multilayer deposition of organics and metals, avoiding electrical disconnections because of topological steps.[19]

Microscale patterns of luminescent CdS particles in the nanocomposite film can be fabricated by scanning the focused laser beam on the sample surface (scheme in the inset of Fig. 2). The fluorescence micrographs of some realized patterns are shown in Fig. 4d–g, displaying features with width of about 1 μm, comparable to the diffraction limited focal spot size ($d_f = 1.22\lambda/NA$, where NA is the objective numerical aperture). For the sake of comparison, we recall that CdS fluorescent lines with 240 μm width are reported by UV-assisted synthesis and patterning.[12b] While sub-diffraction spatial resolution has been reported by two-photon lithography,[17] the resolution limit of these methods has to be evaluated for each specific material system. For our compound, the pattern spatial resolution in the

Fig. 3 (a) HR-TEM image of the nanocomposite after fs laser exposure. Inset: high resolution image of a single particle (mean particle size ≅ 4 nm), showing well pronounced (002) lattice fringes (fringe distance 0.334 nm). Marker = 3 nm. Exposure parameters: incident fluence 0.1 J cm^{-2} and exposure time 5 s. (b) HR-TEM image of some CdS nanocrystals (left side) with the corresponding FFT image (right side). Marker = 5 nm. FFT analysis confirms the wurtzite phase of CdS, showing well pronounced (002) lattice fringes (fringe distance 0.334 nm).
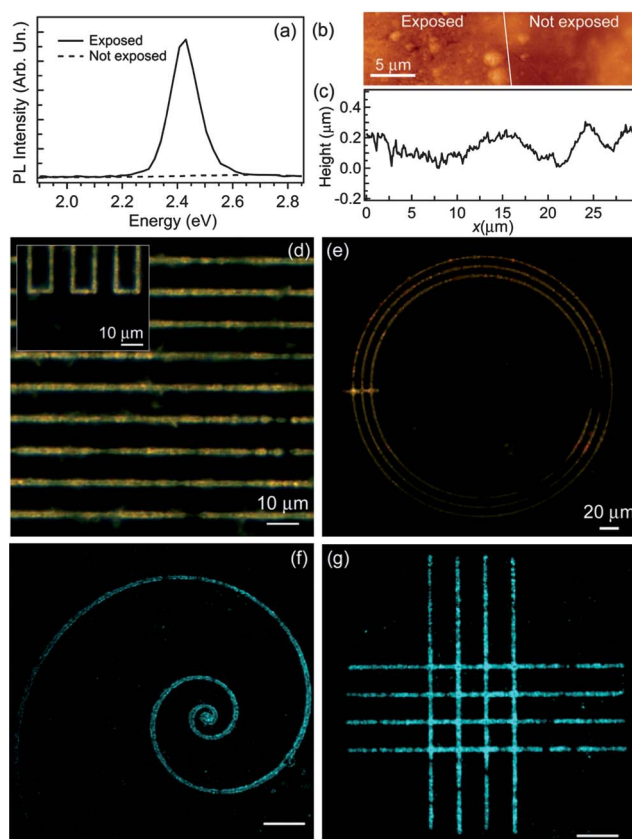
TOPAS®–C12 films is mainly limited by scattering of incident laser light by the aggregated structures formed by the precursors (Fig. 1), blurring the focal spot size.

Among processes possibly involved in the CdS growth, multi-photon absorption of C12 can induce the photolysis of the precursor and the consequent crystal nucleation. This mechanism would be analogous to UV-assisted synthesis, in which the resonant absorption of light induces the decomposition of the precursors and the nucleation of particles.[12] In addition, a contribution from a local temperature increase due to multi-photon absorption of either the polymer matrix or the precursor cannot be ruled out. Indeed, annealing temperature enabling the synthesis of CdS nanoparticles from C12 (230–275 °C[9b]) is compatible with local heating as measured in polymeric systems under experimental conditions similar to those here employed.[20]

Nanocomposite emission properties

To investigate the emission properties of the nanocomposites more in depth, we explore the possibility of tailoring the PL by controlling the particle size through a proper choice of the process parameters. As well-known, excitons confined along lengths (D) comparable to the Bohr radius ($D \approx 2a_B$) exhibit a "quantum size effect", increasing their band gap energy upon decreasing D.[21,22] For CdS, $a_B \cong 3$ nm, and confinement effects on the band gap energy are reported for particles with diameter $D < 9$ nm.[23] Fig. 5 displays the PL spectra of our nanocomposites upon exposure to laser radiation at different fluences. The broad
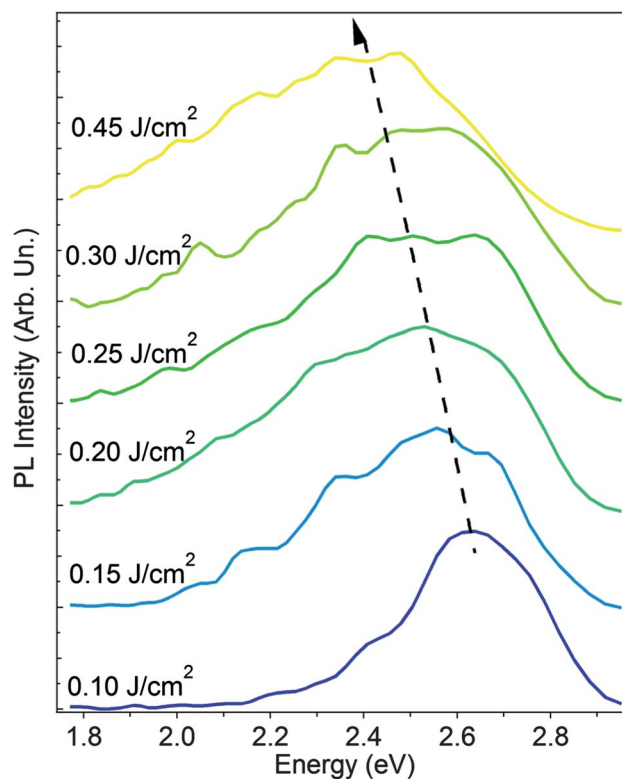

Fig. 5 PL spectra of the nanocomposite, upon exposure by different laser fluences. From bottom to top: 0.10, 0.15, 0.20, 0.25, 0.30, and 0.45 J cm^{-2}. The spectra are vertically shifted for better clarity. The dashed line is a guide for the eyes.
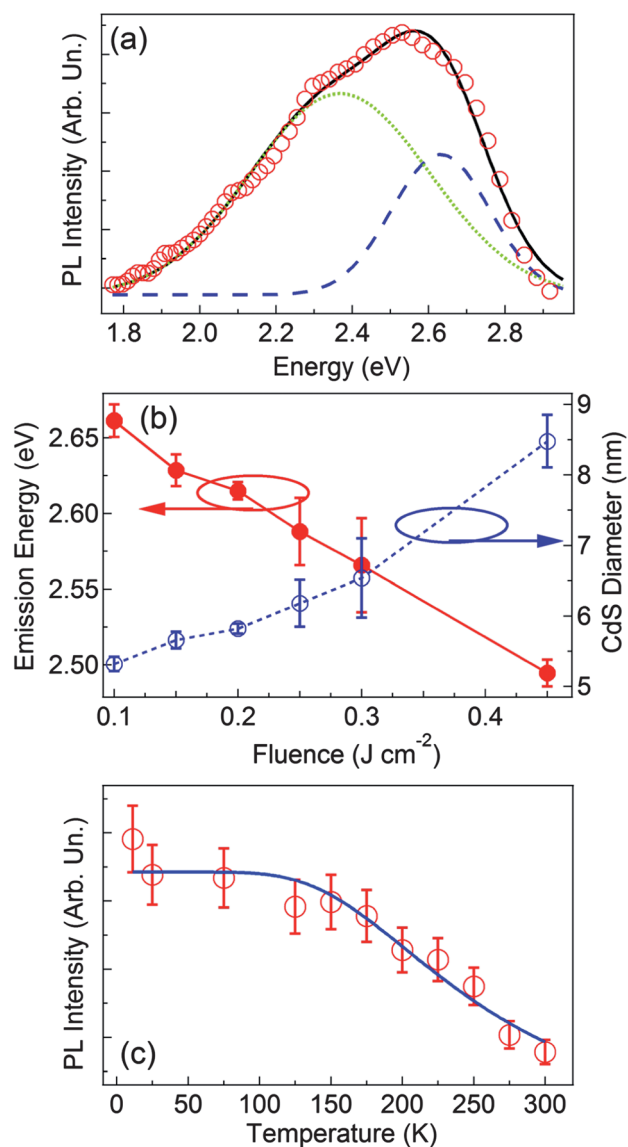
emission exhibits a peak energy red-shifted from about 2.7 eV to about 1.8 eV upon increasing the exposure fluence from 0.10 to 0.45 J cm^{-2}. As typical of CdS nanoparticles, the PL can be ascribed to a superposition of different contributions. The bulk exciton emission is peaked at 2.4–2.43 eV,[14,21] whereas a shift to higher energies of the exciton emission is observed upon reducing the nanoparticle size.[23] Moreover, due to the nanoparticle high surface-area-to-volume ratio, emission from surface trap states is often observed, with spectral features depending on the synthesis method, the storage conditions and the exposure to air or oxygen.[12a,24] Emission from defects typically occurs around 2.3 eV for shallow defects and at about 2 eV for deep trap states. Therefore, the here observed nanocomposite spectra are attributed to the superposition of two main contributes, i.e. a band edge exciton and defect emission for energies above or below 2.4 eV, respectively. We find that the ratio between the PL intensity at lower energies and the excitonic emission intensity is enhanced by about a factor of 6 upon increasing fluence, because of the correspondingly larger expected density of defects.[12b,25]

In order to better elucidate the effect of the irradiation fluence, these two contributions are deconvoluted by fitting the spectra with two Gaussian functions (Fig. 6a). This analysis evidences a decrease of band gap energy from 2.67 to 2.48 eV upon increasing the fluence up to 0.45 J cm^{-2} (Fig. 6b), thus demonstrating the possibility of tuning the nanocomposite emission. Furthermore, from the band-edge emission peak energy one can infer the average particle size taking into account the effective mass approximation in the quantum confinement regime:[26,27]

$$E_{np} = E_G + \frac{2\hbar^2\pi^2}{D^2}\left(\frac{1}{m_e^*} + \frac{1}{m_h^*}\right) - 1.786\frac{2e^2}{\varepsilon D} \qquad (1)$$

In the previous equation, E_{np} is the CdS nanoparticle energy gap, E_G is the bulk energy gap, m_e^* and m_h^* are the effective mass of electrons and holes, respectively, and ε is the CdS dielectric constant. The average particle sizes, obtained by eqn (1) and the measured E_{np} values, range from 5 to 9 nm (Fig. 6b), which overlaps consistently with HRTEM data. These results demonstrate that multi-photon in situ synthesis allows tailoring the optical properties of the CdS nanocrystals by changing the laser beam properties, in particular the incident photon flux. By increasing the laser fluence, a larger number of precursor molecules can be decomposed due to the intensity dependence of the multi-photon absorption process.[28] The light absorption is likely to induce the C–S bond photolysis and the cleavage of the pristine lamellar structure, followed by a decrease of the Cd and S atom separation (also favoured by a local increase of the temperature following the non-linear absorption of the incident light).[20] This mechanism initiates the nanocrystals nucleation, similarly to the thermal assisted in situ synthesis in TOPAS®–C12 films.[9b] The increase of incident fluence makes this process more efficient, finally leading to CdS nanocrystals with larger diameters. Moreover, at the highest fluences (>0.3 J cm^{-2}) a larger number of unsaturated S atoms can be generated,[12] thus increasing the amount of nanocrystal surface defects and their trap state emission. This can be characterized by a decrease of intensity, I_{PL}, observed upon increasing the temperature, T, according to thermally activated processes, as described by the following expression:[29]

This journal is © The Royal Society of Chemistry 2012

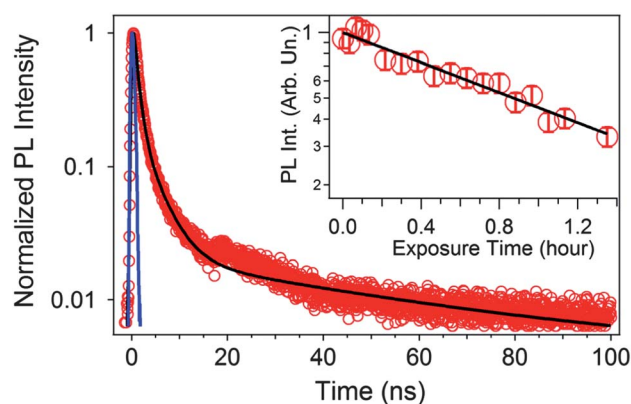J. Mater. Chem., 2012, **22**, 9787–9793 | 9791

Fig. 7 Time evolution of the nanocomposite emission. The black continuous line is a fit to the data by the sum of three exponential functions, convoluted with the instrumental response function, displayed as a blue continuous line. Inset: PL decay upon continuous exposure to UV pumping light. The black solid line is a fit to the data by an exponential function.

of the PL is characterized by the presence of components with different emission lifetimes. By fitting the data with the sum of three exponential functions, we find the presence of a major component (60–80%) with a fast decay time (<1 ns, that is the time resolution of the used system), a second component with a lifetime of a few ns (about 20–40%) and a minor component (<2%) with a long lifetime (>20 ns). These findings are compatible with emission from band-edge and deep trap states.[30]

Finally, the photo-stability of the nanocomposite is evaluated, by measuring the quenching of the emission of the obtained CdS nanoparticles, upon continuous exposure to a pulsed laser beam ($\lambda = 355$ nm, fluence ≈ 100 μJ cm^{-2}, pulse width 2 ns), in air (the inset of Fig. 7). The data are well described by an exponential decay with a lifetime ($1/e$) of about 1.5 hours, corresponding to about 10^5 laser pulses, comparable to other emitting nanomaterials under similar excitation conditions.[3,31]

Conclusions

We demonstrate the *in situ* synthesis of CdS fluorescent nanoparticles in a transparent polymer matrix by near infrared fs-laser pulses. HRTEM and PL analyses evidence the formation of CdS nanocrystals with diameter $D > 4$ nm. The peak emission from the quantum-sized nanoparticles can be tuned from 2.48 to 2.67 eV by changing the incident laser fluence in the range 0.10–0.45 J cm^{-2}. By scanning the near infrared laser, fluorescent patterns can be realized in the nanocomposite material with micrometric resolution, opening up perspectives for application in microstructured and pixelated hybrid light-emitting devices.

Acknowledgements

Fig. 6 (a) PL spectrum of the nanocomposite, upon exposure with an incident fluence of 0.20 J cm^{-2} (empty circles), together with its fit by the sum of two Gaussian functions (continuous line). These correspond to exciton emission (dashed line) and trap state emission (dotted line), respectively. (b) Emission peak energy of the excitonic component (solid circles, left vertical scale) and diameter of the CdS nanoparticles (empty circles, right vertical scale), calculated by using eqn (1), *vs.* incident laser fluence. (c) Temperature dependence of the PL intensity for a nanocomposite obtained by a fluence of 0.4 J cm^{-2}. The continuous line is a fit to the data by eqn (2).

$$I_{PL} = A/\left(1 + Be^{-E_a/k_BT}\right) \qquad (2)$$

where A and B are constants, k_B is the Boltzmann constant and E_a is the activation energy. In Fig. 6c we display the temperature dependence of the emission of the nanocomposite synthesized at a fluence of 0.4 J cm^{-2}, whose data are in agreement with this expected behavior. An activation energy of about 70 meV is indeed estimated, by fitting the data of Fig. 6c to eqn (2), a value comparable to other studies on CdS nanocrystals.[29] The origin of the emission in the nanocomposite synthesized by laser exposure is also confirmed by the time resolved PL data (Fig. 7). The decay

Notes and references

1 (a) K. E. Gonsalves, L. Merhari, H. Wu and Y. Hu, *Adv. Mater.*, 2001, **13**, 703; (b) C. Sanchez, B. Lebeau, F. Chaput and J.-P. Boilot, *Adv. Mater.*, 2003, **15**, 1969; (c) A. A. R. Neves, A. Camposeo, R. Cingolani and D. Pisignano, *Adv. Funct. Mater.*, 2008, **18**, 751; (d) L. D. Carlos, R. A. S. Ferreira, V. de Zea Bermudez and S. J. L. Ribeiro, *Adv. Mater.*, 2009, **21**, 509; (e) C. Minelli, S. B. Lowe and M. M. Stevens, *Small*, 2010, **6**, 2336.

2 X. Duan, Y. Huang, R. Agarwal and C. M. Lieber, *Nature*, 2003, **421**, 241.

3 Y. Chan, J. S. Steckel, P. T. Snee, J. M. Caruge, J. M. Hodgkiss, D. G. Nocera and M. G. Bawendi, *Appl. Phys. Lett.*, 2005, **86**, 073102.

4 (a) G. Zhu, Z. Cheng, T. Lv, L. Pan, Q. Zhao and Z. Sun, *Nanoscale*, 2010, **2**, 129; (b) Y.-L. Lee and Y.-S. Lo, *Adv. Funct. Mater.*, 2009, **19**, 604.

5 C.-H. Chou, H.-S. Wang, K.-H. Wei and J. Y. Huang, *Adv. Funct. Mater.*, 2006, **16**, 909.

6 H. Zhang, J. Han and B. Yang, *Adv. Funct. Mater.*, 2010, **20**, 1533.

7 Z. Tang, Y. Geng, J. W. Y. Lam, B. Li, X. Jing, X. Wang, F. Wang, A. B. Pakhomov and X. X. Zhang, *Chem. Mater.*, 1999, **11**, 1581.

8 S. S. Shankar, S. Chatterjee and M. Sastry, *PhysChemComm*, 2003, **6**, 36.

9 (a) W. S. Rees and G. Kräuter, *J. Mater. Res.*, 1996, **11**, 3005; (b) T. Di Luccio, A. M. Laera, L. Tapfer, S. Kempter, R. Kraus and B. Nickel, *J. Phys. Chem. B*, 2006, **110**, 12603; (c) H. C. Leventis, S. P. King, A. Sudlow, M. S. Hill, K. C. Molloy and S. A. Haque, *Nano Lett.*, 2010, **10**, 1253; (d) F. Di Benedetto, A. Camposeo, L. Persano, A. M. Laera, E. Piscopiello, R. Cingolani, L. Tapfer and D. Pisignano, *Nanoscale*, 2011, **3**, 4234.

10 (a) H. Du, G. Q. Xu, W. S. Chin, L. Huang and W. Ji, *Chem. Mater.*, 2002, **14**, 4473; (b) T. Cui, J. Zhang, J. Wang, F. Cui, W. Chen, F. Xu, Z. Wang, K. Zhang and B. Yang, *Adv. Funct. Mater.*, 2005, **15**, 481.

11 (a) Y. Yin, X. Xu, X. Ge, C. Xia and Z. Zhang, *Chem. Commun.*, 1998, 164; (b) D. Wu, X. Ge, Z. Zhang, M. Wang and S. Zhang, *Langmuir*, 2004, **20**, 5192.

12 (a) A. Athanassiou, R. Cingolani, E. Tsiranidou, C. Fotakis, A. M. Laera, E. Piscopiello and L. Tapfer, *Appl. Phys. Lett.*, 2007, **91**, 153108; (b) D. Fragouli, V. Resta, P. P. Pompa, A. M. Laera, G. Caputo, L. Tapfer, R. Cingolani and A. Athanassiou, *Nanotechnology*, 2009, **20**, 155302.

13 H. Wang, P. Fang, Z. Chen and S. Wang, *Appl. Surf. Sci.*, 2007, **253**, 8495.

14 H. Tong and Y. J. Zhu, *Nanotechnology*, 2006, **17**, 845.

15 L. Persano, S. Molle, S. Girardo, A. A. R. Neves, A. Camposeo, R. Stabile, R. Cingolani and D. Pisignano, *Adv. Funct. Mater.*, 2008, **18**, 2692.

16 Z. B. Sun, X. Z. Dong, W. Q. Chen, S. Nakanishi, X. M. Duan and S. Kawata, *Adv. Mater.*, 2008, **20**, 914.

17 S. Kawata, H. B. Sun, T. Tanaka and K. Takada, *Nature*, 2001, **412**, 697.

18 (a) T. Nielsen, D. Nilsson, F. Bundgaard, P. Shi, P. Szabo, O. Geschke and A. Kristensen, *J. Vac. Sci. Technol., B*, 2004, **22**, 1770; (b) L. Caprioli, E. Mele, F. E. Angilè, S. Girardo, A. Athanassiou, A. Camposeo, R. Cingolani and D. Pisignano, *Appl. Phys. Lett.*, 2007, **91**, 113113.

19 R. Stabile, A. Camposeo, L. Persano, S. Tavazzi, R. Cingolani and D. Pisignano, *Appl. Phys. Lett.*, 2007, **91**, 101110.

20 D. Day and M. Gu, *Opt. Express*, 2005, **13**, 5939.

21 N. Pinna, K. Weiss, J. Urban and M. P. Pileni, *Adv. Mater.*, 2001, **13**, 261.

22 A. P. Alivisatos, *J. Phys. Chem.*, 1996, **100**, 13226.

23 (a) T. Vossmeyer, L. Katsikas, M. Giersig, I. G. Popovic, K. Diesner, A. Chemseddine, A. Eychmüller and H. Weller, *J. Phys. Chem.*, 1994, **98**, 7665; (b) B. Yang, J. E. Schneeloch, Z. Pan, M. Furis and M. Achermann, *Phys. Rev. B: Condens. Matter Mater. Phys.*, 2010, **81**, 073401.

24 (a) K. K. Nanda and S. N. Sahu, *Solid State Commun.*, 1999, **111**, 671; (b) C.-W. Wang and M. G. Moffit, *Langmuir*, 2004, **20**, 11784; (c) R. Premachandran, S. Banerjee, V. T. John, G. L. McPherson, J. A. Akkara and D. L. Kaplan, *Chem. Mater.*, 1997, **9**, 1342.

25 We observe emission spectra dominated by excitonic emission, with small contribution by defect emission, in less than 10% of the analysed sample areas.

26 L. Efros and A. L. Efros, *Sov. Phys. Semiconduct.*, 1982, **16**, 772.

27 L. E. Brus, *J. Chem. Phys.*, 1983, **79**, 5566.

28 G. S. He, L. S. Tan, Q. Zheng and P. N. Prasad, *Chem. Rev.*, 2008, **108**, 1245.

29 S. Santhi, E. Bernstein and F. Paille, *J. Lumin.*, 2006, **117**, 101.

30 F. Wu, J. Z. Zhang, R. Kho and R. K. Mehra, *Chem. Phys. Lett.*, 2000, **330**, 237.

31 (a) J. R. Lakowicz, I. Gryczynski, Z. Gryczynski and C. J. Murphy, *J. Phys. Chem. B*, 1999, **103**, 7613; (b) E. V. Klyachkovskaya, S. V. Vashchenko, A. P. Stupak and S. V. Gaponenko, *J. Appl. Spectrosc.*, 2010, **77**, 732.